geosciences

MDPI

Article

UAV, GNSS, and GIS for the Rapid Assessment of Multi-Occurrence Landslides

Konstantinos G. Nikolakopoulos *, Aggeliki Kyriou and Ioannis K. Koukouvelas

Department of Geology, University of Patras, 26504 Patras, Greece; a.kyriou@ac.upatras.gr (A.K.); iannis@upatras.gr (I.K.K.)

* Correspondence: knikolakop@upatras.gr

Abstract: Intense long-duration rainfall or extreme precipitation in a few hours can provoke many simultaneous shallow landslides. In the past, the term multi-occurrence regional landslides (MORLEs) was proposed to describe such phenomena. In the current study, unmanned aerial vehicles in combination with a global navigation satellite system sensor and geographical information systems seem to be the ideal solution for the rapid assessment of many landslides occurring in Aitoloakarnania Prefecture, Western Greece. Fourteen landslides were accurately mapped within a few working days, and precise orthophotos and reports were created and submitted to the local authorities. The analysis of meteorological data proved that there is a peak in precipitation height that triggers the MORLEs in the specific area. Specifically, the value of the daily precipitation was defined at 80 mm.

Keywords: landslide; UAV; precipitation; MORLEs

check for updates

Citation: Nikolakopoulos, K.G.; Kyriou, A.; Koukouvelas, I.K. UAV, GNSS, and GIS for the Rapid Assessment of Multi-Occurrence Landslides. *Geosciences* **2024**, *14*, 160. https://doi.org/10.3390/geosciences14060160

Academic Editors: Jesus Martinez-Frias, Matteo Del Soldato, Roberto Tomás, Anna Barra and Davide Festa

Received: 25 April 2024
Revised: 31 May 2024
Accepted: 7 June 2024
Published: 9 June 2024

Copyright: © 2024 by the authors. Licensee MDPI, Basel, Switzerland. This article is an open access article distributed under the terms and conditions of the Creative Commons Attribution (CC BY) license (https://creativecommons.org/licenses/by/4.0/).

1. Introduction

Landslides, worldwide, annually cause the loss of hundreds of millions of euros in damage [1] and thousands of fatalities [2]. The number of global human losses due to landslides surpassed 55,997 deaths between 2004 and 2016 [2]. In the same study, it was proven that there has been an important growth in the number of fatal landslide events in one hundred and twenty-eight countries around the world during the last twenty years. Landslides are often triggered by regional phenomena (earthquakes, typhoons), resulting in damage at the regional scale. Such landslides may provoke loss of energy power or communication, infrastructure isolation caused by blocked or destroyed transportation networks, and severe delays to emergency responses. Even small, isolated landslides affecting a central highway of railway network may be turned into an economic disaster. It is also commonplace that there is a significant spatial and temporal correlation between the occurrence of deadly landslides and earlier intense precipitation events [3]. Nevertheless, most of the deadliest landslide events in history are a sequence of multiple landslides with the same trigger [4]. The term multi-occurrence landslides was first proposed in 2005 [5]. The proposed term, multi-occurrence regional landslide events (MORLEs) [5,6], refers to a great number of shallow landslides taking place almost simultaneously within determined areas, ranging from tens to more than thousands of square kilometers. Shallow landslides are debris-flow slides triggered by precipitation events with short duration and high intensity or with long duration and medium–low intensity [7,8]. Such slides act on soil of low thickness (up to 2 m), originating from the weathering of the bedrock. This specific type of landslide usually occurs without any warning signs in unstable landslide-prone areas; therefore, they are impossible for researchers to predict and quite difficult to monitor. Furthermore, shallow landslides triggered by precipitation extremes may cause considerable damage or human loss [7,9,10].

MORLEs have been observed in several countries worldwide. From historical data, thirteen MORLEs have been recorded in the broader area of Catalonia in the last one hundred and twenty years. The range of these landslides varies between ten and twenty

thousand square kilometers [11]. The common triggering factor of these thirteen events was the intense rainfall. In addition, a typhoon named Mangkhut caused one thousand one hundred and one landslides in the Itogon region of the Philippines in 2018. The total extent of the landslides exceeded 570 square kilometers [12]. A few years ago, in 2011, another typhoon named Talas was the triggering factor for the occurrence of MORLEs in Japan [13]. More than eighteen landslides were mapped in the broader area, including a slide in the Shizuoka prefecture, located almost 400 km away from the main typhoon track [14]. Moreover, an extreme precipitation event (the highest daily precipitation of 200 years) was recorded on 30 July 2019 in Norway. As a result, dozens of debris flows occurred. Among them, five were characterized as large events, with a volume ranging between ten and twenty-five cubic meters, while more than forty smaller debris flows were also mapped [15]. Generally speaking, multi-spectral remote sensing data (Sentinel-2), the digital elevation model (ALOS), and classification algorithms have been used to detect MORLEs [16].

Many recent research studies have focused on the use of unmanned aerial vehicles (UAVs) for landslide mapping and monitoring [17–25]. Chou et al. [17] have taken advantage of the ability of UAVs to access unsafe landslide areas for the purposes of disaster management. UAV imagery was collected in order to analyze the overall environmental change caused by the MORAKOT typhoon (2009) in Taiwan. Many landslides in unstable and/or inaccessible sites were mapped using UAVs, and the produced 3D data were compared with previous elevation models. The new possibilities that come from the combination of UAVs and structure from motion (SfM) photogrammetry for the periodic monitoring and temporal evolution of shallow landslides have been demonstrated [18]. The combination of UAVs photogrammetry, GNSS measurements, and the installation of permanent pillars inside the landslide body has been proven to be very efficient in assessing the slide evolution, even throughout the fast movement stage, and in calculating the slide velocity [19]. According to [20], the use of UAVs present many advantages in the daily monitoring of landslides, such as rapidity, high accuracy, and economic affordability. The processing of imagery acquired on three repeated UAV flight campaigns from 2017 to 2019 with ground control points measured with GNSS produced 3D data and allowed for detailed mapping of the debris flow [21]. In a similar study, geodetic and topographic measurements of high precision were blended with the use of UAV imagery in order to monitor the surface movement in an urban area in Romania [22]. In two studies [23,24], the same research team proved that it is feasible to accurately co-register multi-temporal UAV datasets, to determine landslide surface dynamics, and to calculate volumetric differences from the multi-temporal DSMs created by UAV data. In another study, the dynamic of landslides on a reservoir bank was assessed using a combination of UAV, TLS, GNSS data, and GIS techniques [25]. In general, there are many studies demonstrating the flexibility and efficiency of the low-cost UAVs with RGB cameras in landslide investigations [26–31].

The current study focuses on the combined use of unmanned aerial vehicles (UAVs), global navigation satellite systems (GNSS), and geographical information systems (GIS) for the rapid assessment of MORLEs in the Aitoloakarnania prefecture in Western Greece. Two MORLEs events have been recorded in the specific area in 2021. The advantages of UAV imagery over satellite remote sensing data for the accurate mapping of the damage are also presented. A further analysis has been performed on the meteorological conditions during these events, and the precipitation threshold that triggers the landslides has been identified. The main asset of such work is that it is implemented for the first time in Greek territory, while the utilization of UAV-based data for the research of such phenomena is also innovative at the international level since existing works focus mainly on the documentation of MORLEs using conventional approaches.

2. Study Area and Geological Background

The broader area affected by the MORLEs is included in the municipality of Agrinio in Aitoloakarnania prefecture, Western Greece. Eight villages spread over the entire area of

the municipality (1.247 km^2) were affected by the landslides. The location of these villages, as well as the extent of the municipality, are presented in Figure 1.

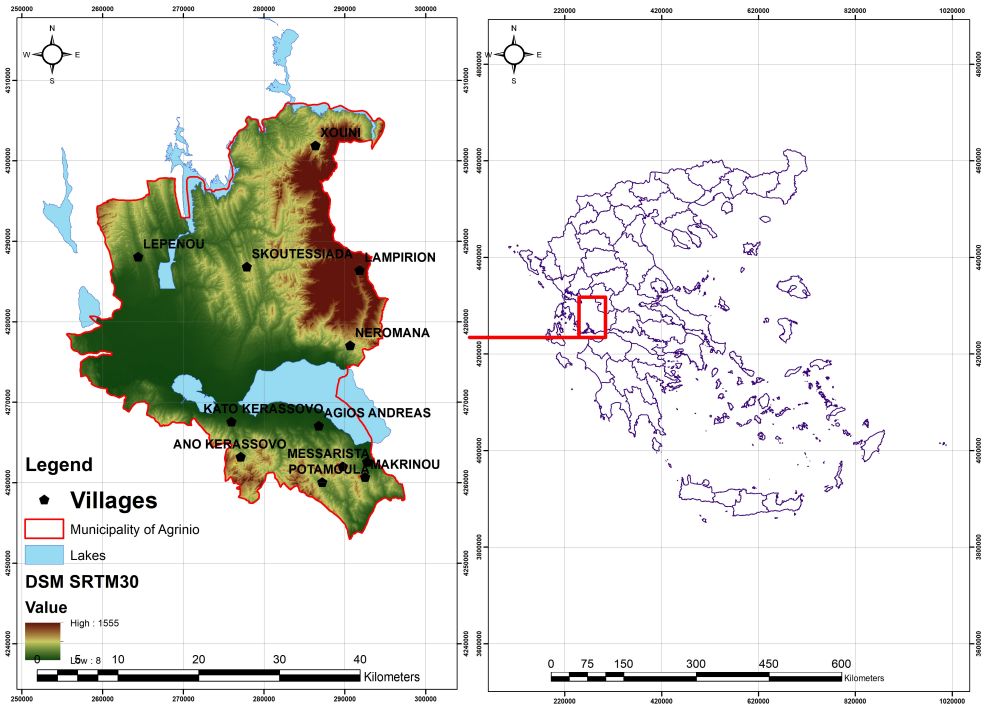


Figure 1. Area of multi-landslide occurrence in 2021.

The area where the landslides are mapped is located on the outskirts of the Pindos Mountain range in the east and the east bluff of the Arakynthos Mountain in the west. This study area belongs to two geotectonic units: the Pindos in the east and the Ionian unit in the west. The contact between these two units is one of the most important geological structures through the Hellenides mountain chain, called the Pindos Thrust [32]. The Pindos Thrust is a crustal-scale thrust transporting rocks of the Pindos unit towards the west. Thus, the study area is characterized by geological complexity, and the landslides develop through different geological conditions. Two major triggering factors of landslides in the Pindos unit are lithology and structure. Pindos unit lithology includes a Late Cretaceous-Paleocene flysch sequence composed of sandstones, marls, and clay shales; Late Cretaceous limestones; Jurassic–Lower Cretaceous schist–chert formation with intercalations of cherts; and siliceous and earthy clays, along with thin plated limestones. The sedimentary formations of the unit develop primarily a relatively thin soil horizon less than a meter thick. In addition, flysch, in the unit, is composed of different rhythmic alternations of competent/strong sandstone layers with low-strength siltstone/clayey schist beds, favoring landslide triggering. Another landslide-triggering factor in the Pindos unit is the intensive deformation of these rocks. Indeed, the unit was deformed during the Alpine orogeny by a dense array of fault-bend folds, fault-controlled duplexes, and moderate-to-high-angle west-verging thrust faults [32,33]. All these structures show an NNW- to NW-trend and impose high shear deformation in the Pindos unit rocks, as is common and present in other similar geological settings across west Greece. The geomorphology in the east part of the study area is characterized by steep west-facing slopes and deep river incisions. In the west, the Ionian's unit prevailing lithology is Oligocene Arakynthos sandstone, showing sand and clay alternations from place to place. Arakynthos sandstone weathering causes a well-developed zone which ranges from 0.5 to 7 m thick [34]. This thick weathering zone is chaotic in structure, including sandstone fragments within a soil-like matrix. Meteoric water permeability differences through this zone favor shallow landslides. A series of dormant landslides can be recognized throughout the landscape of this flysch.

The structural grain in the Ionian unit is less intense, and the area is deformed by a train of NW-trending open synclines and anticlines. This alpine structural grain is truncated by the Lake Trichonida WNW-trending normal fault. This fault is mapped at the northern end of a series of NW-trending drainage basins, which drain the Ionian unit flysch deposits. A simplified geological map of the broader area is included in the Supplementary Material.

In summary, although heavy rainfall is considered an important factor in triggering landslides over the study area, lithology and structure are also crucial factors in controlling the final development of the landslides in the study area. Based on our analysis, triggering factors like lithology are more important in the west, and inherited structure is more important in the east.

3. Materials and Methods

Three remote sensing datasets were processed to map MORLEs within the area of interest: (a) a digital orthophoto map produced by the Greek Cadastre; (b) a Pleiades multi-spectral image; and (c) unmanned aerial vehicle (UAV) imagery.

In more detail, the Greek Cadastre has produced digital orthophotos covering the whole country during the period 2007–2008. These orthophotos have a spatial resolution of 0.5 m and they are produced from digital airphotos. The specific dataset is usually used as the basemap for change detection studies.

Moreover, Pleiades multi-spectral imagery with the same spatial resolution (0.5 m) was used to detect and map the landslides occurring in December 2021. The image was acquired on 11 May 2022, almost five months after the landslide events. The four bands cover the blue, green, red, and near-infrared part of the spectrum.

On the other hand, UAV flight campaigns were implemented over all the landslides within three weeks after the events. To cover as many sites as possible, we used two different UAVs, i.e., a DJI Phantom 4 Pro V2 and a DJI Matrice 600. Phantom 4 Pro is a quadcopter that can be carried inside the main body of the slide and can take-off in almost any environment. It has a 20 MP camera that can capture images of 5472 $\times$ 3078 pixels. Matrice 600 is a hexacopter equipped with a X5 camera that captures images of 4608 $\times$ 3456 pixels (16 MP). It needs more space for take-off and landing; however, it can cover larger areas. Both cameras have mechanical shutters and thus they exhibit minimum distortions.

All the landslides mapped by UAV imagery were acquired via photogrammetric flight campaigns. The flights were performed at 90–120 m altitude (above ground level). Inside each landslide body, we have distributed many artificial square targets to identify and measure them as ground control points. Each target was measured with a real-time kinematic GNSS receiver with sub-centimeter accuracy. Agisoft Metashape software (v. 2.0.1., Agisoft LLC, St. Petersburg, Russia) was used for the photogrammetric processing of the UAV imagery. The processing methodology has been described in detail in previous studies [35,36]. The digital surface model and orthophoto of each landslide were produced and projected to the Hellenic Geodetic Reference System 1987.

The aforementioned products covering each landslide were imported into a geographic information system (GIS) to measure the extent of the affected areas, map the damage, and compare them to the post-disaster, high-resolution Pleiades imagery, as well as to the pre-disaster orthophoto of the Greek Cadastre.

Furthermore, meteorological measurements from seven stations around the municipality of Agrinio were analyzed. The specific stations are part of the National Observatory of Athens network. There are daily, monthly, and yearly data for the precipitation, the temperature, the wind speed, the wind direction, etc.

4. Multi-Occurrence Landslide Events

4.1. First Event

Heavy rainfall (93.6 mm) on 27 January caused the first three landslides on 28 January 2021 (Table 1). A few days later, on 8 February 2021, our team started the systematic mapping and monitoring of these landslides. Three landslides were mapped using UAV

imagery and in situ measurements with a GNSS sensor (Figure 2). The first landslide destroyed the main road of the village. The slide has 200 m width and 400 m length. It destroyed some warehouses and greenhouses around of the main road. The second landslide took place just outside of the village, affecting a dirty road. The dimensions of the second landslide were mapped in the GIS environment (100 m width, 150 m length). The third landslide severely damaged the main road leading from Kerassovo to Messolonghi. It was a linear slide that was only 80 m width; however, its length surpassed 300 m. It affected three continuous steep turns, as presented in Figure 2.

Table 1. Landslides occurring on 28 January 2021.

No	Study Area	Dimensions	Damage in Buildings
1	Kerassovo inside the village	150 m width, 400 m length	X
2	Kerassovo outside of the village	100 m width, 150 m length	
3	Kerassovo on the road to Messolonghi	80 m width, 250 m length	

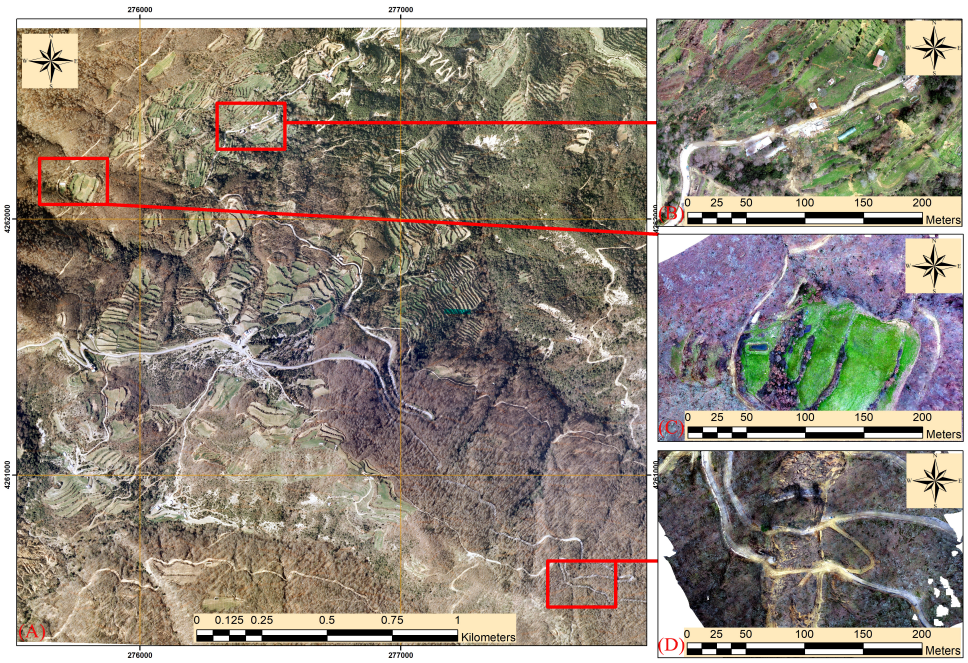


Figure 2. Three landslides occurred in the broader area of Kerassovo village on the night of 20 January 2021: (**A**) the broader area of the village; (**B**) the landslide on the main road; (**C**) the second landslide just outside of the village, affecting cultivations; (**D**) the third landslide that destroyed the main road leading from Kerassovo to Messolonghi.

4.2. Second Event

The second and more severe event happened on 12 December 2021, following the high precipitation of the previous night (86 mm). Sixteen landslides occurred, affecting eight villages inside the boundaries of the Agrinio municipality (Figure 1 and Table 2). In the Agios Andreas area, the landslide destroyed the road just outside the village entrance. Messarista village suffered from five landslides inside and outside the main settlement. The landslides affected an area of 2.5 km width by 1.8 km length. Many buildings inside the village were seriously damaged seriously. The exact dimensions of each landslide are presented in Table 2. At the same time, two landslides, one outside of village and one affecting the main road inside the village, occurred in Ano Makrinou. Inside the village, dozens of buildings incurred serious damage. Moreover, the previous landslide inside Kerassovo village was been reactivated and enlarged. The width of the landslide increased from 150 m in January 2021 to more than 500 m in December 2021. Three houses were

destroyed. Damage also appeared in the infrastructure of three other villages, namely, Ano Vlochos; Lampiri-Rapteika; and Chouni-Sagieika. In Lepenou and Neromana villages, the landslides mainly affected the road network. The dimensions of each landslide are presented in Table 2.

Table 2. Landslides occurred on 5 December 2021.

No	Study Area	Dimensions	Damage in Buildings
1	Agios Andreas	50 m width	
2	Messarista first before the village entrance	100 m width	
3	Messarista second village entrance	150 m width	
4	Messarista third inside the village	250 m width	X
5	Messarista fourth Upper neighborhood	150 m width	X
6	Messarista fifth water pumping building	300 m width	X
7	Messarista sixth after the village	200 m width	
8	Ano Makrionou inside the village	250 m width	X
9	Ano Makrinou outside of the village	70 m width	
10	Ano Kerassovo	500 m width	X
11	Ano Vlochos	100 m–500 m	X
12	Neromana on the main road	50 m width	
13	Neromana second	80 m width	
14	Lampiri—Rapteika	150 m width	X
15	Chouni—Sagieika	100 m width	X
16	Lepenou	50 m width	

Figure 3 presents some indicative photos of the damage incurred by buildings and the road network. Those photos were taken during the field work.



Figure 3. Some characteristic photos of damage to buildings and the road network: (**A**) damage to a house in Kerassovo; (**B**) crack in the backyard of a house in Ano Vlochos; (**C**) a warehouse covered by debris in Makrinou; (**D**) cracks on the wall of a house in Rapteika; (**E**) an entire house that slid in Messarista; (**F**) the main road at Agios Andreas village; (**G**) damage to the main road in Neromana village; (**H**) the main road in Ano Makrinou was severely damaged; and (**I**) a bulldozer cleaning the main road in Ano Vlochos.

5. Damage Mapping

UAV photogrammetric flight campaigns were designed and executed over the landslides. Depending on the landslide extent and the slope, the flight altitude ranged between 80 and 120 m. All the flights were performed with a front overlap ratio of 85% and a side overlap ratio of 75%. More details are presented in Table 3 below.

Table 3. Details of the photogrammetric flight campaigns.

No	Study Area	No of Images Acquired	Altitude	Platform	Spatial Resolution cm
1	Kerassovo inside the village	250	120	P4pro	3.3
2	Kerassovo outside of the village	60	120	P4pro	3.3
3	Kerassovo on the road to Messolonghi	40	110	Matrice 600	2.8
4	Messarista first before the village entrance	90	120	Matrice 600	3.0
5	Messarista second village entrance	95	120	P4pro	3.3
6	Messarista third inside the village	75	110	P4pro	3.0
7	Messarista fourth Upper neighborhood	75	110	P4pro	3.0
8	Messarista fifth water pumping building	140	120	Matrice 600	3.0
9	Messarista sixth after the village	120	120	Matrice 600	3.0
10	Ano Makrionou inside the village	80	120	P4pro	3.3
11	Ano Makrinou outside of the village	90	120	Matrice 600	3.0
12	Ano Vlochos	158	120	P4pro	3.3
13	Lampiri—Rapteika	186	110	Matrice 600	2.8
14	Chouni—Sagieika	60	90	P4pro	2.5

The orthophotos derived from UAV imagery processing were further processed in the ArcMap environment in order to delineate any possible crack that could generate new slides in the future. Each image was compared with the respective orthophoto from the Greek cadastral. In Figure 4, three orthophotos derived from the UAV imagery are compared with the Cadastral basemap of Messarista village. The first orthophoto presents the landslide at the entrance of the village, the second one shows the main landslide in the center of the village, and the third one displays the landslide occurring on the main road at the west of Messarista. The damage to the infrastructures and the road network is easily marked on the UAV imagery. Many cracks were detected and mapped, as can be observed in Figure 4.

Figures 5 and 6 demonstrate the effectiveness of UAV imagery in the assessment of the damage in the case of multi-occurrence landslides. In Figure 5, the basemap of the Greek Cadastral is displayed in comparison to the Pleiades imagery and to the UAV orthophoto. The basemap (Figure 5A), with a spatial resolution of 50 cm, depicts the area of Kerassovo before the landslide. The black line indicates the main road, while the yellow lines define the extent of the landslide event on 11 December 2021. In the Pleiades imagery (Figure 5B), acquired five months after the event, the landslide body is easily detected. The black line indicates the destroyed main road of the village. The specific image also has a spatial resolution of 50 cm, which permits the accurate mapping of the landslide extent. However, only the ultra-high spatial resolution of the UAV imagery (Figure 5C) allows for the mapping of all the small cracks inside the landslide body. As can be observed in Figure 5C, there are hundreds of breaks on the ground from where the water penetrates deeper, which may cause reactivation of the landslide.

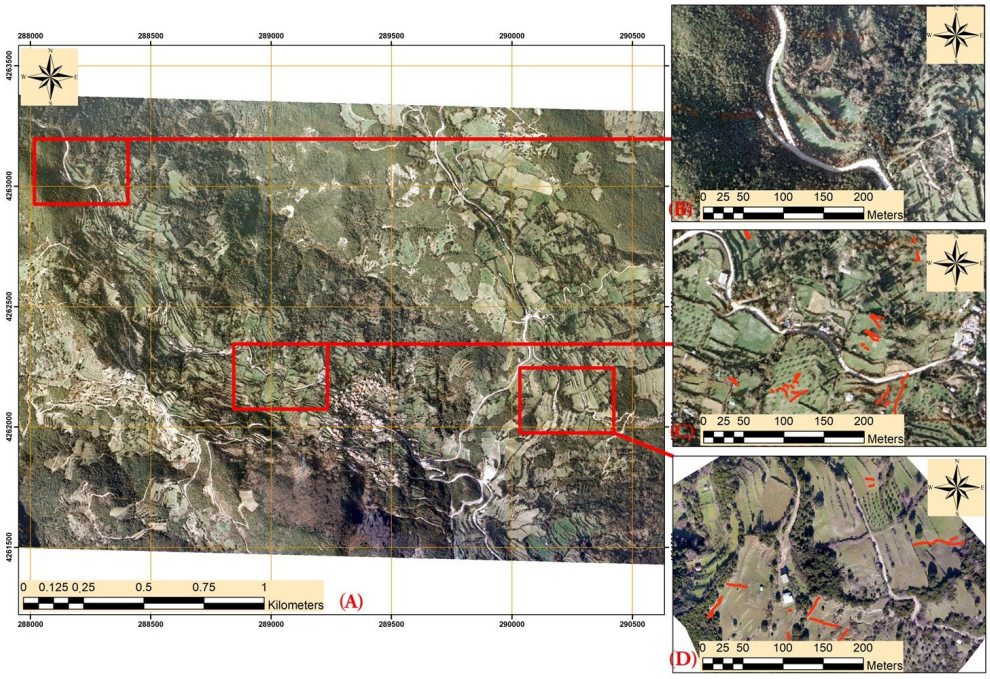


Figure 4. Three of the five landslides that occurred in the broader area of Messarista village on 11 December 2021. (**A**) the basemap of the Greek Cadastre presenting the village before the event. (**B**) UAV orthophoto of the landslide at the village entrance (**C**) UAV orthophoto of third landslide inside the village. (**D**) UAV orthophoto of the fifth landslide near to the water pumping building. Red lines: diverse cracks digitized in the ArcMap environment.

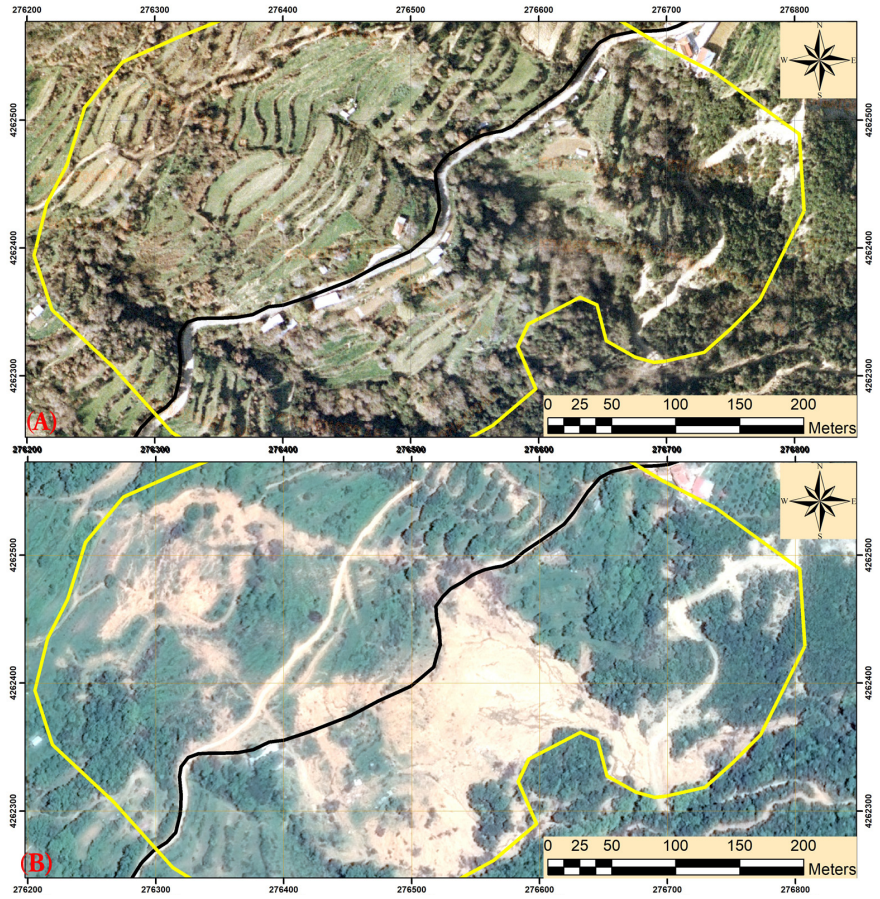


Figure 5. *Cont.*

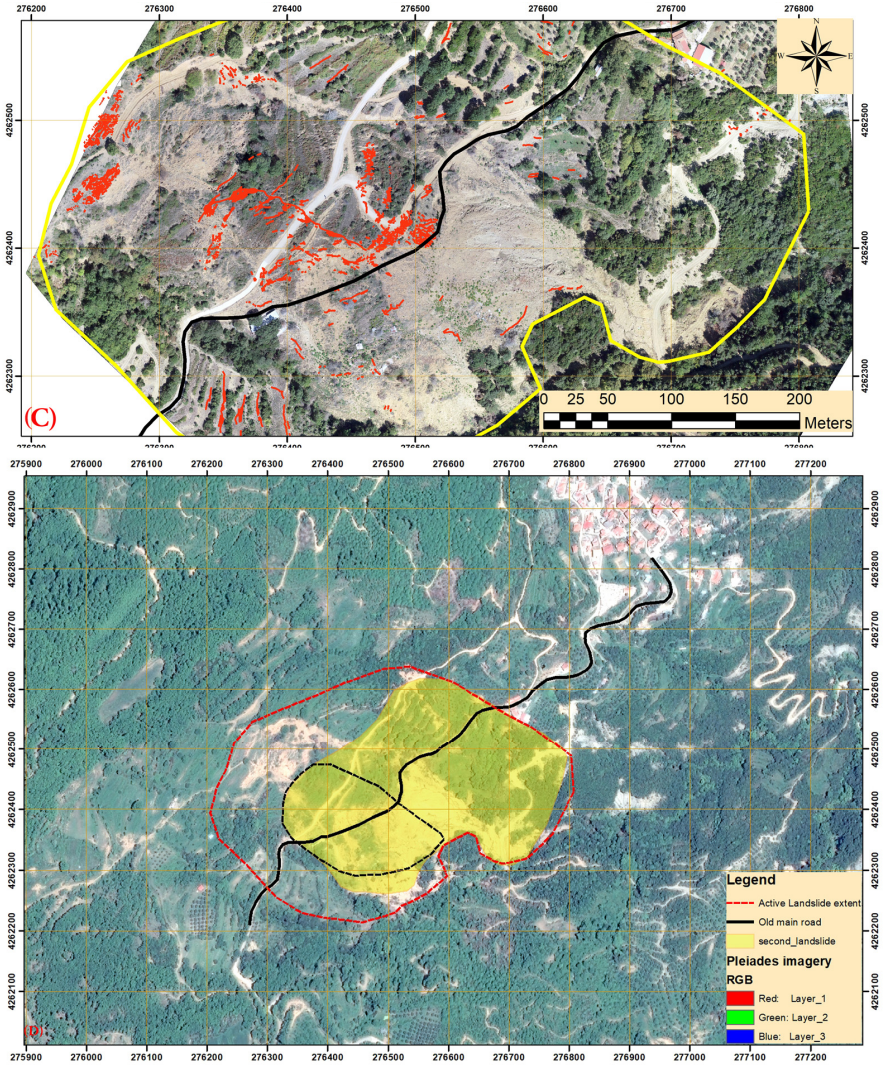


Figure 5. (**A**) The basemap of the Greek Cadastral presents Kerassovo before the landslide; (**B**) the same area from Pleiades imagery; (**C**) the landslide as mapped in the UAV orthophoto (the black line indicates the main road, while the yellow lines define the extent of the landslide event on 11 December 2021); (**D**) a simplified map of the landslide.

The superiority of UAV imagery compared to other remote sensing data, like Pleiades satellite imagery, in the assessment of the MORLEs is presented in Figure 6. At a scale of 1/200, a small part of Messarista village is presented. In Figure 6A, the basemap of the Cadastral displays the area before the landslide. The same area is presented in Figure 6B after the landslide, as captured by Pleiades imagery. In Figure 6C, the UAV orthophoto is depicted. It is very clear that the higher spatial resolution of the UAV data permits the exact mapping and digitization of the damage on the road, as well as any small crack in the fields.

Another advantage of the use of UAVs is the ease, low cost, and immediacy in post disaster mapping. Just after the MORLEs, and under only the prerequisite of the weather conditions, the UAVs can be deployed to map the affected area with great accuracy. Our team exploited the specific characteristics of the UAVs, covering all the areas affected within in the days following the MORLEs phenomenon. Processing the data in the GIS environment helps us to compose a report and inform the local stakeholders about the extent of each landslide, the severity of the damage, and the future risk for each settlement.

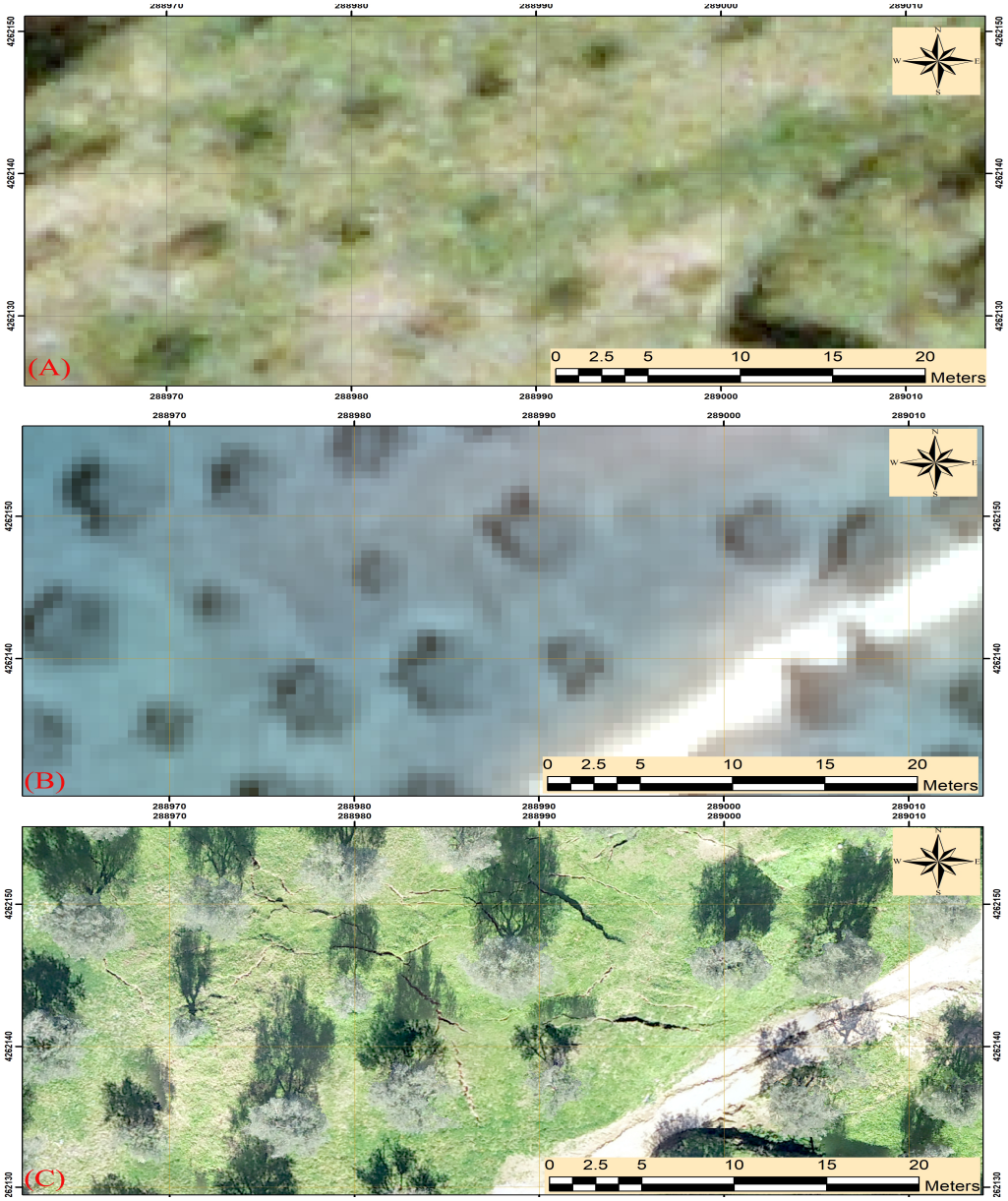


Figure 6. (**A**) The basemap of the Greek Cadastral presents a part of Messarista village before the landslide; (**B**) part of the Pleiades imagery; (**C**) orthophoto from the UAV data. Many cracks in the field and the damage on the road can be easily detected and mapped accurately on the UAV orthophoto.

6. Meteorological Data Analysis and Discussion

To correlate the MORLEs with the precipitation, an analysis of the meteorological data from all the weather stations around the Agrinio municipality was performed. Figure 7 presents the maximum daily rain of seven meteorological stations in January 2021. As can be observed on 26 January 2021, the precipitation reached almost 100 mm in Gavalou station, while 90 mm of rain was measured in Orini Nafpaktia and more than 60 mm of daily rain was observed in the stations of Karpenissi, Amfilochia, and Aitoliko.

Figure 8 presents the respective precipitation values of the same meteorological station on December 2021. As can be observed on 11 December 2021, extreme rain of 160 mm was recorded in Orini Nafpaktia and an extreme of 140 mm was reported in Gavalou station. A total of 110 mm of rain was measured in Karpenissi, and more than 85 mm of daily rain was observed in Agrinio.

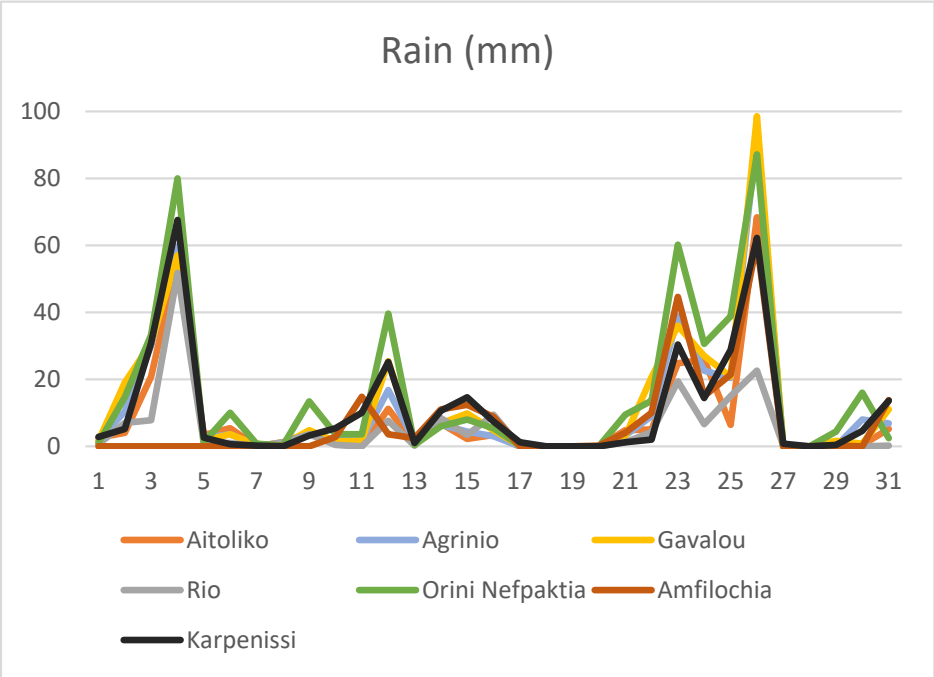


Figure 7. The daily height of rain in January 202, at the seven meteorological stations around the Agrinio municipality.

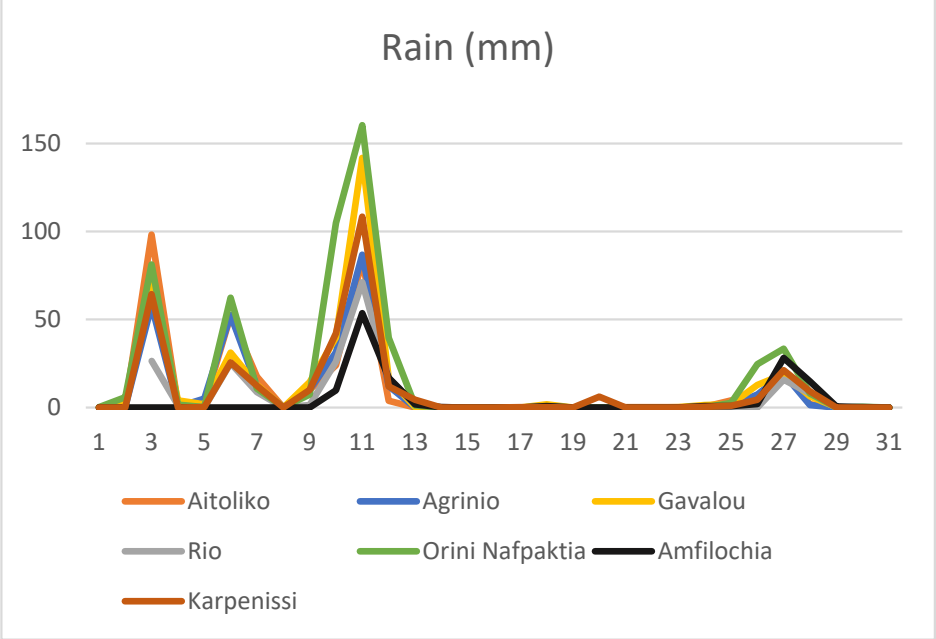


Figure 8. The daily height of rain in December 2021 at the seven meteorological stations around the Agrinio municipality.

Those values of maximum daily precipitation can be characterized as extremes. As can be observed in Figure 9, the accumulated rain high in January 2021 is 390 mm in Gavalou station. The observed precipitation maximum of 100 mm on 26 January is almost one third of the monthly total rain. On 11 December 2021, the daily maximum rain height reached 140 mm, while the monthly total rain is 382 mm. The specific daily maximum can be characterized as extreme as it represents 36% of the total monthly precipitation.

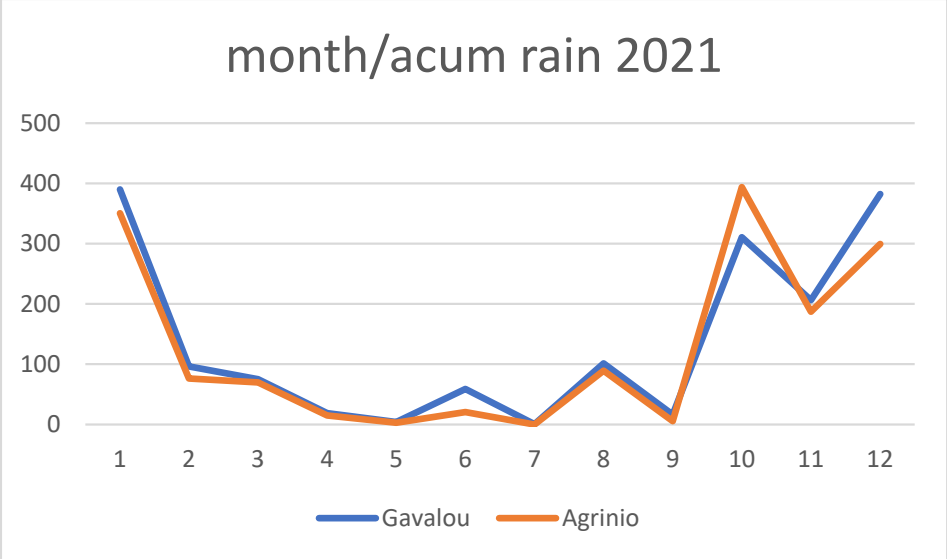


Figure 9. The total precipitation per month for 2021 as measured in the meteorological stations of Agrinio and Gavalou.

Lake Trichonida is located in the middle of the Agrinio municipality. The villages of Ano and Kato Kerassovo, Makrinou, Messarista, Neromana, and Agios Andreas are located at the south of Lake Trichonida. According to the spatial distribution of the precipitation (Figures 10 and 11), a local maximum of precipitation is observed over those villages, while Lake Trichonida seems to represent a physical barrier, accelerating the rainfall extremes at the southern part. Specifically, the rainfall in this local region varied between 80 and 100 mm on 25 January 2021 (Figure 10) and between 100 and 140 mm on 11 December 2021 (Figure 11).

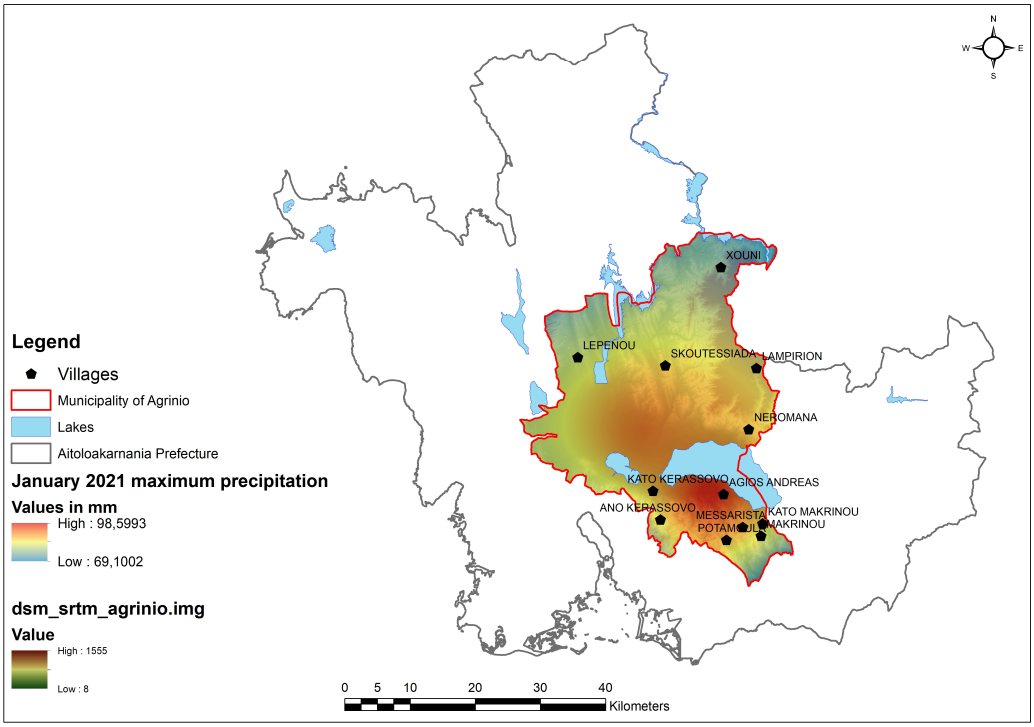


Figure 10. The spatial distribution of precipitation high during the first MORLEs event on 26 January 2021.

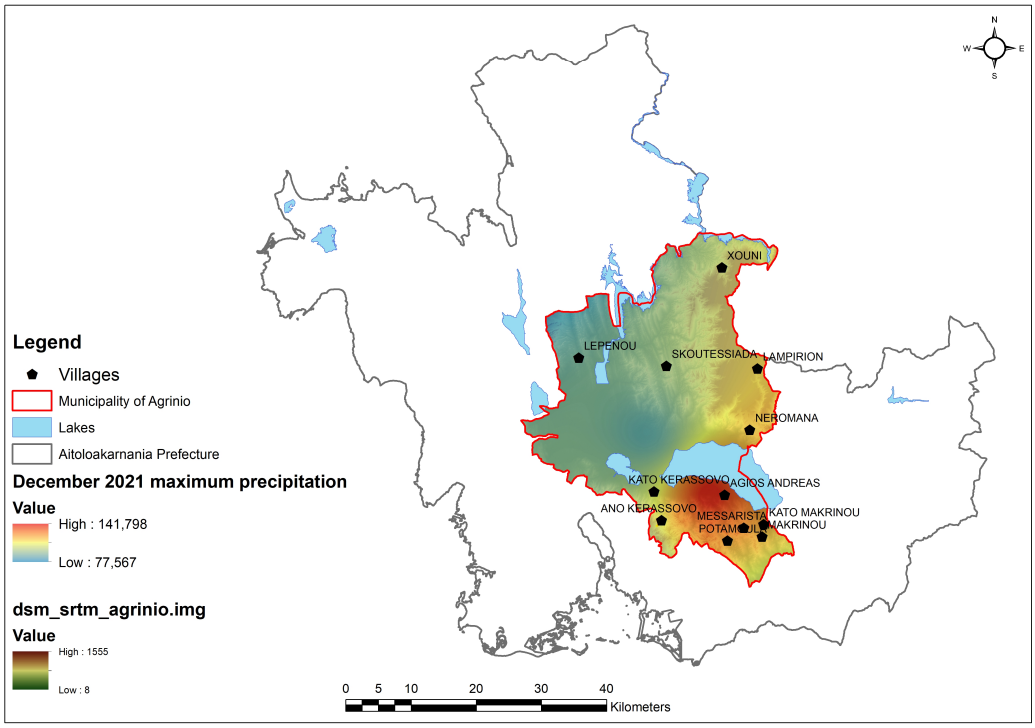


Figure 11. The spatial distribution of precipitation high during the second MORLEs event on 11 December 2021.

Multiple-occurrence regional landslide events are triggered by extreme precipitation events and can be very destructive and dangerous as there is no kind of previous alert. Thus, it is very important to define the rainfall thresholds or peaks that can potentially be used as the basis for a multi-stage early warning system in civil protection procedures [37]. The specific study registered the MORLEs phenomenon for the first time in Western Greece and tried to define such a threshold. This is in accordance with more sophisticated efforts to define debris flows rainfall thresholds in Italy [37,38]. Similar phenomena have been mentioned in another study for Crete Island [39] in 2019. In Figure 12A,B, we present two diagrams of the humidity, the temperature, and the precipitation measured at the meteorological station of Agrinio for the period 1956–2010. As can be observed in Figure 12A, the relative humidity in the broader area is quite high and ranges between 70% and 80% during the winter. This is probably due to the existence of the lakes across the municipality. At the same time, the lower temperatures (Figure 12B) during the winter period range between 3.4 and 5 degrees Celsius. The mean temperature for the winter period ranges between 8.3 and 9.6 degrees Celsius. It is obvious that there is no high snowfall and snow coverage in the specific area. The precipitation presents high values (Figure 12B) in January and February and very high values on November and December. In the first two months of the year, the monthly precipitation surpassed 100 mm, while in November and December, it surpassed 150 mm. Figure 12C presents the precipitation peaks during the period 2018–2023 in comparison to the mean precipitation value for the period 1956–2010. The positive values prove that the precipitation has surpassed the mean value of the period 1956–2010, while the negative values mark less rain than usual. As can be observed in January 2019 and 2021, there is a peak in precipitation values (213 mm and 219 mm more rain than usual, respectively), while the mean precipitation value in January for the period 1956–2010 is 114.7 mm. A similar peak is observed in December 2021, when the precipitation value is 204 mm higher than the mean precipitation value in December for the period 1974–2010 (114.7 mm).

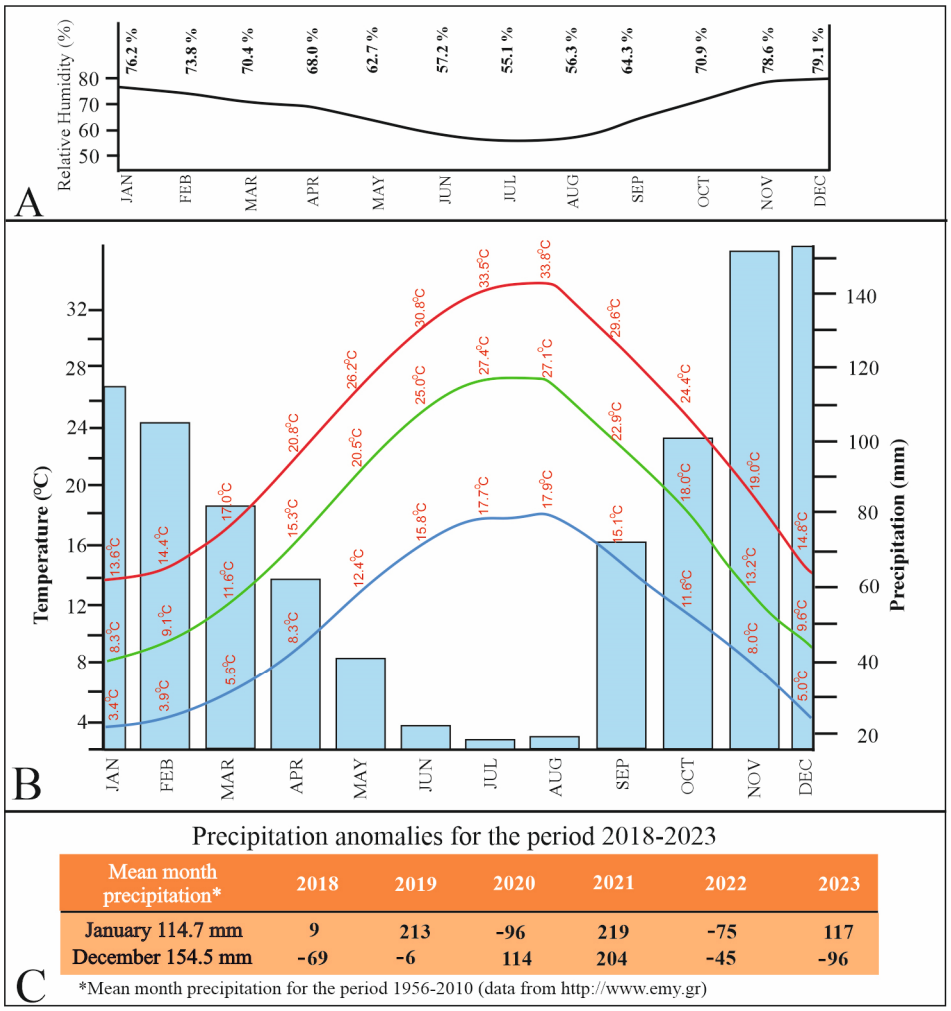


Figure 12. (**A**) The relative monthly humidity for the period 1956–2010; (**B**) precipitation and minimum, mean, and maximum temperature for the same period; (**C**) precipitation peaks during the 2018–2023 period.

A comparison of the daily precipitation values in January 2021 (Figure 7) and December 2021 (Figure 8), the monthly accumulated precipitation value (Figure 9), and the mean monthly precipitation value (Figure 12C) lead to the conclusion that we had two extreme rain peaks in 2021 that triggered the multi-occurrence regional landslides in the Agrinio municipality.

7. Conclusions

This specific study investigates the phenomenon of multi-occurrence regional landslides in the prefecture of Aitoloakarnania, Western Greece. In this framework, UAV flights were executed to map the affected areas and assess the damage. Pleiades imagery and an orthophoto derived from the Greek Cadastral were utilized to facilitate our investigations. The main findings of the research are summarized in the following:

- It was proven that there is a threshold in precipitation height that triggers the MORLEs in the specific area. Specifically, the value of the daily precipitation was detected at 80 mm. This was the daily rainfall peak of 21 January, while the respective threshold of 21 December is somewhat higher, reaching 140 mm.
- In general, it was mentioned that in the specific year under study, there were two precipitation peaks in January and December in comparison to the mean precipitation values for the period 1956–2010.

- Satellite data with very high spatial resolution, such as Pleiades, can be used for the MORLEs mapping; however, these data are quite expensive and acquired only on demand. UAV imagery is the most effective solution for the rapid assessment of such phenomena when the number of the landslides is high and their extent is limited.
- The combination of UAV, GNSS, and GIS is proposed for the accurate mapping of the damage and the provision of crucial information to the local stakeholders.

In the future, we plan to monitor such areas systematically in order to better understand the triggering factors and the sliding mechanisms. Deeper analysis of the meteorological data is needed in order to more accurately define the MORLEs' precipitation threshold.

Supplementary Materials: The following supporting information can be downloaded at: https://www.mdpi.com/article/10.3390/geosciences14060160/s1.

Author Contributions: Conceptualization, K.G.N.; methodology, K.G.N., A.K. and I.K.K.; software, A.K. and K.G.N.; validation, K.G.N., A.K. and I.K.K.; writing—original draft preparation, K.G.N.; writing—review and editing K.G.N., A.K. and I.K.K.; project administration, K.G.N. All authors have read and agreed to the published version of the manuscript.

Funding: This research received no external funding.

Data Availability Statement: Data collected during the field work are available upon request to the corresponding author.

Conflicts of Interest: The authors declare no conflicts of interest.

References

1. Clague, J.J.; Stead, D. (Eds.) *Landslides: Types, Mechanisms and Modeling*; Cambridge University Press: Cambridge, UK, 2012. [CrossRef]
2. Froude, M.J.; Petley, D. Global fatal landslide occurrence from 2004 to 2016. *Nat. Hazards Earth Syst. Sci.* **2018**, *18*, 2161–2181. [CrossRef]
3. Haque, U.; da Silva, P.F.; Devoli, G.; Pilz, J.; Zhao, B.; Khaloua, A.; Wilopo, W.; Andersen, P.; Lu, P.; Lee, J.; et al. The human cost of global warming: Deadly landslides and their triggers (1995–2014). *Sci. Total Environ.* **2019**, *682*, 673–684. [CrossRef] [PubMed]
4. The Deadliest Landslides In Recorded History. Available online: https://www.worldatlas.com/natural-disasters/the-deadliest-landslides-in-recorded-history.html (accessed on 6 June 2024).
5. Crozier, M.J. Multiple-occurrence regional landslide events in New Zealand: Hazard management issues. *Landslides* **2005**, *2*, 247–256. [CrossRef]
6. Crozier, M.J. Reprint of "A proposed cell model for multiple-occurrence regional landslide events: Implications for landslide susceptibility mapping". *Geomorphology* **2018**, *307*, 3–11. [CrossRef]
7. Caine, N. The Rainfall Intensity—Duration Control of Shallow Landslides and Debris Flows. *Geogr. Ann. Ser. A Phys. Geogr.* **1980**, *62*, 23–27. [CrossRef]
8. Giannecchini, R.; Galanti, Y.; D'Amato Avanzi, G. Critical rainfall thresholds for triggering shallow landslides in the Serchio River Valley (Tuscany, Italy). *Nat. Hazards Earth Syst. Sci.* **2012**, *12*, 829–842. [CrossRef]
9. Guzzetti, F.; Peruccacci, S.; Rossi, M.; Stark, C.P. Rainfall thresholds for the initiation of landslides in central and southern Europe. *Meteorol. Atmos. Phys.* **2007**, *98*, 239–267. [CrossRef]
10. Hungr, O.; Leroueil, S.; Picarelli, L. The Varnes classification of landslide types, an update. *Landslides* **2014**, *11*, 167–194. [CrossRef]
11. Buxó, P.; Oller, P.; Xifré, D.; Fabregat, I.; Marturià, J.; Janeras, M. Identification, validation and assessment of Multiple Occurrence Regional Landslide Events (MORLE) in Catalonia (Spain) during the last one hundred years. In Proceedings of the EGU General Assembly 2021, Online, 19–30 April 2021; EGU21-6171. [CrossRef]
12. Abancó, C.; Bennett, G.L.; Matthews, A.J.; Matera, M.A.M.; Tan, F.J. The role of geomorphology, rainfall and soil moisture in the occurrence of landslides triggered by 2018 Typhoon Mangkhut in the Philippines. *Nat. Hazards Earth Syst. Sci.* **2021**, *21*, 1531–1550. [CrossRef]
13. Yamada, M.; Matsushi, Y.; Chigira, M.; Mori, J. Seismic recordings of landslides caused by Typhoon Talas (2011), Japan. *Geophys. Res. Lett.* **2012**, *39*, 1–5. [CrossRef]
14. Okuwaki, R.; Fan, W.; Yamada, M.; Osawa, H.; Wright, T.J. Identifying landslides from continuous seismic surface waves: A case study of multiple small-scale landslides triggered by Typhoon Talas, 2011. *Geophys. J. Int.* **2021**, *226*, 729–741. [CrossRef]
15. Rouault, C. Extreme Multiple Landslide Events in Norway An Investigation of Rainfall and Snowmelt Induced Soil Landslide Detection and Forecasting. Master's Thesis, Cold Climate Engineering, Norwegian University of Science and Technology, Faculty of Engineering, Department of Civil and Environmental Engineering, Trondheim, Norway, 2020.
16. Tehrani, F.S.; Santinelli, G.; Herrera, M.H. Multi-Regional landslide detection using combined unsupervised and supervised machine learning. *Geomat. Nat. Hazards Risk* **2021**, *12*, 1015–1038. [CrossRef]

17. Chou, T.-Y.; Yeh, M.-L.; Chen, Y.-C.; Chen, Y.-H. Disaster monitoring and management by the unmanned aerial vehicle technology. In Proceedings of the ISPRS TC VII Symposium—100 Years ISPRS, Vienna, Austria, 5–7 July 2010.
18. Casagli, N.; Frodella, W.; Morelli, S.; Tofani, V.; Ciampalini, A.; Intrieri, E.; Raspini, F.; Rossi, G.; Tanteri, L.; Lu, P. Spaceborne, UAV and ground-based remote sensing techniques for landslide mapping, monitoring and early warning. *Geoenviron. Disasters* **2017**, *4*, 9. [CrossRef]
19. Ciccarese, G.; Tondo, M.; Mulas, M.; Bertolini, G.; Corsini, A. Rapid Assessment of Landslide Dynamics by UAV-RTK Repeated Surveys Using Ground Targets: The Ca' Lita Landslide (Northern Apennines, Italy). *Remote Sens.* **2024**, *16*, 1032. [CrossRef]
20. Godone, D.; Allasia, P.; Borrelli, L.; Gullà, G. UAV and Structure from Motion Approach to Monitor the Maierato Landslide Evolution. *Remote Sens.* **2020**, *12*, 1039. [CrossRef]
21. Notti, D.; Giordan, D.; Cina, A.; Manzino, A.; Maschio, P.; Bendea, I.H. Debris Flow and Rockslide Analysis with Advanced Photogrammetry Techniques Based on High-Resolution RPAS Data. Ponte Formazza Case Study (NW Alps). *Remote Sens.* **2021**, *13*, 1797. [CrossRef]
22. Sestras, P.; Bilașco, Ș.; Roșca, S.; Dudic, B.; Hysa, A.; Spalević, V. Geodetic and UAV Monitoring in the Sustainable Management of Shallow Landslides and Erosion of a Susceptible Urban Environment. *Remote Sens.* **2021**, *13*, 385. [CrossRef]
23. Lucieer, A.; de Jong, S.M.; Turner, D. Mapping landslide displacements using Structure from Motion (SfM) and image correlation of multi-temporal UAV photography. *Progress Phys. Geogr. Earth Environ.* **2014**, *38*, 97–116. [CrossRef]
24. Turner, D.; Lucieer, A.; De Jong, S.M. Time Series Analysis of Landslide Dynamics Using an Unmanned Aerial Vehicle (UAV). *Remote Sens.* **2015**, *7*, 1736–1757. [CrossRef]
25. Yermolaev, O.; Usmanov, B.; Gafurov, A.; Poesen, J.; Vedeneeva, E.; Lisetskii, F.; Nicu, I.C. Assessment of Shoreline Transformation Rates and Landslide Monitoring on the Bank of Kuibyshev Reservoir (Russia) Using Multi-Source Data. *Remote Sens.* **2021**, *13*, 4214. [CrossRef]
26. Rau, J.; Jhan, J.; Lo, C.; Lin, Y. Landslide mapping using imagery acquired by a fixed-wing UAV. *Int. Arch. Photogramm. Remote Sens. Spat. Inf. Sci.* **2011**, *38*, 195–200. [CrossRef]
27. Shi, B.; Liu, C. UAV for landslide mapping and deformation analysis. In Proceedings of the International Conference on Intelligent Earth Observing and Applications, Guilin, China, 23–24 October 2015; International Society for Optics and Photonics: Bellingham, WA, USA, 2015; Volume 9808. [CrossRef]
28. Peternel, T.; Kumelj, Š.; Oštir, K.; Komac, M. Monitoring the Potoška planina landslide (NW Slovenia) using UAV photogrammetry and tachymetric measurements. *Landslides* **2017**, *14*, 395–406. [CrossRef]
29. Cignetti, M.; Godone, D.; Wrzesniak, A.; Giordan, D. Structure from motion multisource application for landslide characterization and monitoring: The champlas du col case study, sestriere, North-Western Italy. *Sensors* **2019**, *19*, 2364. [CrossRef]
30. Antoine, R.; Lopez, T.; Tanguy, M.; Lissak, C.; Gailler, L.; Labazuy, P.; Fauchard, C. Geoscientists in the sky: Unmanned aerial vehicles responding to geohazards. *Surv. Geophys.* **2020**, *41*, 1285–1321. [CrossRef]
31. Catani, F. Landslide detection by deep learning of non-nadiral and crowdsourced optical images. *Landslides* **2020**, *18*, 1025–1044. [CrossRef]
32. Doutsos, T.; Koukouvelas, I.K.; Xypolias, P. A new orogenic model for the External Hellenides. *Geol. Soc. Lond. Spec. Publ.* **2006**, *260*, 507–520. [CrossRef]
33. Skourlis, K.; Doutsos, T. The Pindos Fold-and-thrust belt (Greece): Inversion kinematics of a passive continental margin. *Int. J. Earth Sci.* **2003**, *92*, 891–903. [CrossRef]
34. Nikolakopoulos, K.G.; Kyriou, A.; Koukouvelas, I.K.; Tomaras, N.; Lyros, E. UAV, GNSS, and InSAR Data Analyses for Landslide Monitoring in a Mountainous Village in Western Greece. *Remote Sens.* **2023**, *15*, 2870. [CrossRef]
35. Nikolakopoulos, K.G.; Kyriou, A.; Koukouvelas, I.K. Developing a Guideline of Unmanned Aerial Vehicle's Acquisition Geometry for Landslide Mapping and Monitoring. *Appl. Sci.* **2022**, *12*, 4598. [CrossRef]
36. Kyriou, A.; Nikolakopoulos, K.; Koukouvelas, I. How Image Acquisition Geometry of UAV Campaigns Affects the Derived Products and Their Accuracy in Areas with Complex Geomorphology. *ISPRS Int. J. Geo-Inf.* **2021**, *10*, 408. [CrossRef]
37. Ciccarese, G.; Mulas, M.; Alberoni, P.P.; Truffelli, G.; Corsini, A. Debris flows rainfall thresholds in the Apennines of Emilia-Romagna (Italy) derived by the analysis of recent severe rainstorms events and regional meteorological data. *Geomorphology* **2020**, *358*, 107097. [CrossRef]
38. Ciccarese, G.; Mulas, M.; Corsini, A. Combining spatial modelling and regionalization of rainfall thresholds for debris flows hazard mapping in the Emilia-Romagna Apennines (Italy). *Landslides* **2021**, *18*, 3513–3529. [CrossRef]
39. Argyriou, A.V.; Polykretis, C.; Teeuw, R.M.; Papadopoulos, N. Geoinformatic Analysis of Rainfall-Triggered Landslides in Crete (Greece) Based on Spatial Detection and Hazard Mapping. *Sustainability* **2022**, *14*, 3956. [CrossRef]

Disclaimer/Publisher's Note: The statements, opinions and data contained in all publications are solely those of the individual author(s) and contributor(s) and not of MDPI and/or the editor(s). MDPI and/or the editor(s) disclaim responsibility for any injury to people or property resulting from any ideas, methods, instructions or products referred to in the content.